Electrooptic Mapping and Finite-Element Modeling of the Near-Field Pattern of a Microstrip Patch Antenna

Kyoung Yang, *Student Member, IEEE*, Gerhard David, *Member, IEEE*, Jong-Gwan Yook, *Member, IEEE*, Ioannis Papapolymerou, Linda P. B. Katehi, *Fellow, IEEE*, and John F. Whitaker, *Member, IEEE*

***Abstract*—A comprehensive electrooptic field-mapping technique is applied to the characterization of near-field radiation patterns above a microstrip patch antenna. The amplitude and phase maps of three orthogonal electric-field components, measured using electrooptic crystals above the patch, also have revealed the transition from the near field to the far field of the radiation pattern. In addition, experimental results have been compared with a finite-element method (FEM) simulation. The measurements show superior results to the FEM simulation, especially in terms of spatial resolution and data acquisition times. Furthermore, the scattering parameter S_{11} for the patch antenna has been calculated from the electrooptic measurement results of standing waves on the feeding line and compared with results from a conventional network analyzer.**

***Index Terms*—Electrooptic sampling, microstrip patch antenna, near-field radiation patterns.**

I. Introduction

ELECTROMAGNETIC field probes are used for a variety of applications in microwave metrology where knowledge of electric-field structure is required. These include such diverse areas as the characterization of near-field patterns of antennas and antenna arrays, verification of electromagnetic compatibility (EMC) of electronic equipment, and failure diagnosis of microelectronic integrated circuits. Mainly techniques using dipole- or monopole-type probes [1]–[3] have been pursued, although the optically based technique of electrooptic sampling [4], [5] has also been investigated. Features that make the electrooptic technique very promising are high bandwidth (into the terahertz regime when using ultrashort-pulse lasers) and a spatial resolution on the order of the size of the laser beam diameter or even less. For the typical visible or infrared lasers, the resolution of the electrooptic measurement system can, thus, reach several micrometers. Furthermore, electrooptic sampling does not require that electrodes or ground planes be incorporated as part of the probe so that, compared with conventional probes, the invasiveness of an electrooptic probe is minimal.

Electrooptic measurements can be divided into two schemes, with the implementation depending on the device-under-test (DUT). For microwave structures fabricated on substrates that exhibit linear electrooptic effects, such as GaAs and InP, the internal electrooptic sampling method has proven to be quite effective [6]–[8]. If the substrate does not exhibit such an electrooptic effect and, moreover, when radiation field patterns are to be investigated, it is necessary to utilize external electrooptic sampling. The external electrooptic sampling technique has been employed successfully to obtain two-dimensional field maps that greatly facilitate the characterization of integrated microwave circuits, including the isolation of faults from the interior of a circuit [9]. Electrooptic measurements of the near-field radiation patterns of antennas have also been reported [10], [11]. However, previous work has mainly concentrated on one-dimensional scans or the acquisition of only two field components in the near-field pattern. Any determination of the S-parameters of the antennas has also relied upon additional characterization using a conventional network analyzer.

In this paper, measurements of all three orthogonal electric-field components are demonstrated for a microstrip patch antenna that is designed to have a 4-GHz resonance frequency. The measurements are carried out using two different miniaturized probe crystals that have a cross-sectional area at their tips that is 5–10 times smaller than that of conventional electrooptic probes. Thus, the invasiveness of the probes to the DUT is minimized. Measurements include a near- to far-field transition that has yet to be reported until now, as well as near-field amplitude and phase measurements of the complete patch-antenna radiation pattern. For comparison, a three-dimensional finite-element method (FEM) simulation has been performed for the investigated antenna structure. Even though electrooptic measurement results are found to be superior to the FEM simulation results in terms of spatial resolution and data acquisition time, the measurement and simulation show good agreement. In addition, the scattering parameter S_{11} of the antenna is calculated from the electrooptic field map data, revealing the standing-wave characteristics of the structure at different frequencies. Finally, these results extracted from the electrooptic field measurements are compared with the S_{11} from a conventional network analyzer.

Manuscript received March 4, 1999. This work was supported by the Army Research Office Multidisciplinary University Research Initiative "Spatial and Quasi-Optic Power Combining Program" under Grant DAAG 55-97-0132, by Clemson University under a subcontract, and by the National Science Foundation, Center for Ultrafast Optical Science under STC PHY 8920108. The work of G. David was supported under a Feodor–Lynen Fellowship of the Alexander von Humboldt Foundation.

K. Yang, G. David, L. P. B. Katehi, and J. F. Whitaker are with the Center for Ultrafast Optical Science and Radiation Laboratory, Department of Electrical Engineering and Computer Science, The University of Michigan at Ann Arbor, Ann Arbor, MI 48109-2122 USA (e-mail: whitaker@engin.umich.edu).

J.-G. Yook is with the Kwang-Ju Institute of Science and Technology Kwang-Ju, Korea.

I. Papapolymerou is with the University of Arizona, Tucson, AZ 85721 USA.

Publisher Item Identifier S 0018-9480(00)00841-3.

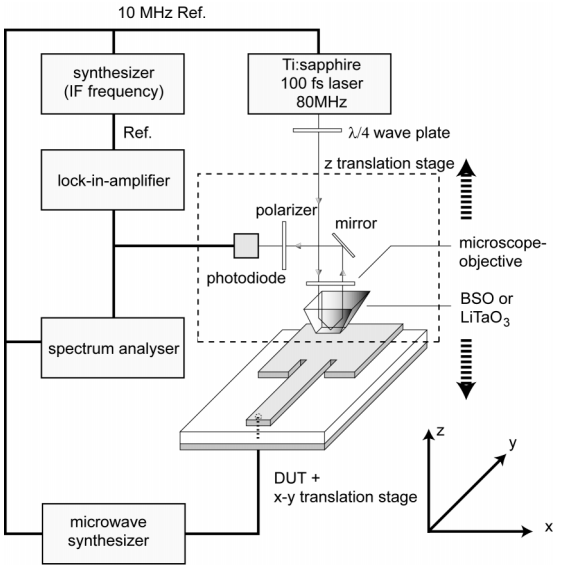

Fig. 1. Electrooptic measurement schematic. See text for further explanation.

II. Measurement System Configuration

The experimental measurement system used is shown in Fig. 1. The optical beam from a phase-stabilized Ti : Sapphire laser, which has 100-fs duration pulse output at an 80-MHz pulse repetition rate, is focused inside of the electrooptic probe crystal. The faces of the probe crystal are polished in order to achieve total internal reflection of the incident beam, which is detected by a photo diode. The reflected beam is analyzed to determine the change of its polarization state, which is sensitive to the RF electric field that extends into the probe crystal. The electrical signal from the photodiode, which is then proportional to the optical signal modulated by the RF electric field in the electrooptic crystal, is measured in a harmonic mixing scheme [4] at an intermediate frequency of several megahertz using an RF lock-in amplifier or a spectrum analyzer. The IF signal is derived from the difference between the input signal frequency and an integer harmonic of the 80-MHz repetition rate. Using phase-locked-loop electronics in the stabilized laser system, one is able to synchronize the CW signal from a microwave synthesizer to the laser pulse train, with the small offset frequency providing the time delay for the sampling gate. Measurements in amplitude and phase are then performed simultaneously as the computer reads the output of the two channels of the lock-in amplifier, which uses the output of a low-frequency synthesizer, also synchronized to the laser electronics, to maintain a phase reference.

The two types of electrooptic probes utilized in this study are fabricated from bismuth silicate (BSO) and lithium tantalate ($LiTaO_3$). While both crystals serve to modulate the laser pulses using an electric field that is parallel to their optic axis, the electrooptic properties of the two materials are different. As a result, BSO is sensitive to normal RF fields that are parallel to the laser path, while $LiTaO_3$ senses the tangential RF fields orthogonal to the light beam in the probe [12], [13]. These materials are chosen for their high electrooptic coefficients and transparency to the wavelength of the Ti : sapphire laser used. Employing the two different types of electrooptic crystals allows the determination of the normal and tangential electric-field components above the antenna under test. The crystals have a tip area of 40 μm ×40 μm for the BSO and 20 μm × 10 μm for the $LiTaO_3$.

The antenna is mounted on a computer-controlled x–y translation stage. In addition to the two-dimensional movement of the DUT, several optical components have freedom of movement in the vertical direction (i.e., those components shown in the dashed box of Fig. 1), so that one may achieve a three-dimensional field-mapping capability. The minimum detectable power emanating from the patch is measured to be about −45 dBm, where it corresponds to a field strength at the probe of approximately 30 V/m, and the sensitivity of the measurement system is 40 mV/$\sqrt{\text{Hz}}$. Typical field-mapping measurements, in which the probe stops for 300 ms at each of 6400 points in the x–y plane so that the lock-in can extract amplitude and phase values, are carried out in approximately 45 min for each height above the antenna that the field is mapped. This data acquisition time has been further reduced since the measurements reported here were made, to as little as 15 min, through the use of a new dc-servo x–y translation stage.

The microstrip patch antenna that served as the DUT was designed for a resonance frequency of 4 GHz. The antenna has 15-μm-thick Cu metallization on both sides of a 2.55-mm-thick Duroid substrate that has a dielectric constant of 10.3. The dimension of the antenna is 8 mm along the x-direction and 11.18 mm in the y-direction (Fig. 1). Also, impedance matching insets, which have 0.5-mm width and 6.1-mm length, are fabricated along the feed line. The backside coaxial feeding method is employed for the antenna, as depicted in Fig. 1. The center conductor of the feeding coaxial cable is connected to the antenna through the 2.2-mm-wide and 34-mm-long microstrip line.

III. Results

A. Three-Dimensional Electrooptic Field Mapping

Fig. 2 shows the amplitude of three orthogonal electric-field components at two different detection heights, with the perimeter of the antenna superimposed to indicate the position of the metal patch. The direction of each component corresponds to the axes shown in Fig. 1. The left-hand-side column of Fig. 2(a) depicts the measured amplitudes for the three components at a reference level of 0 mm, which is actually just above the antenna at a distance approximately 100 μm from its surface. Each amplitude plot is normalized independently so that the maximum field within the scanned area is set to a value of 1.0. Due to the different properties of the electrooptic crystals and the current lack of satisfactory calibration standards for electrooptic sampling, there is also no connection between the field strengths for the tangential and normal components. However, it is observed that the technique clearly allows us to determine the behavior of each component of the electric field in the near field of the patch.

Since the length of the antenna (along the y-direction) is designed to be a half-wavelength at the resonance frequency, the potential reaches its maximum value at the edges of the patch close to the feed line and at the farthest extent from the feed. Following the potential distribution, the maximum electric field

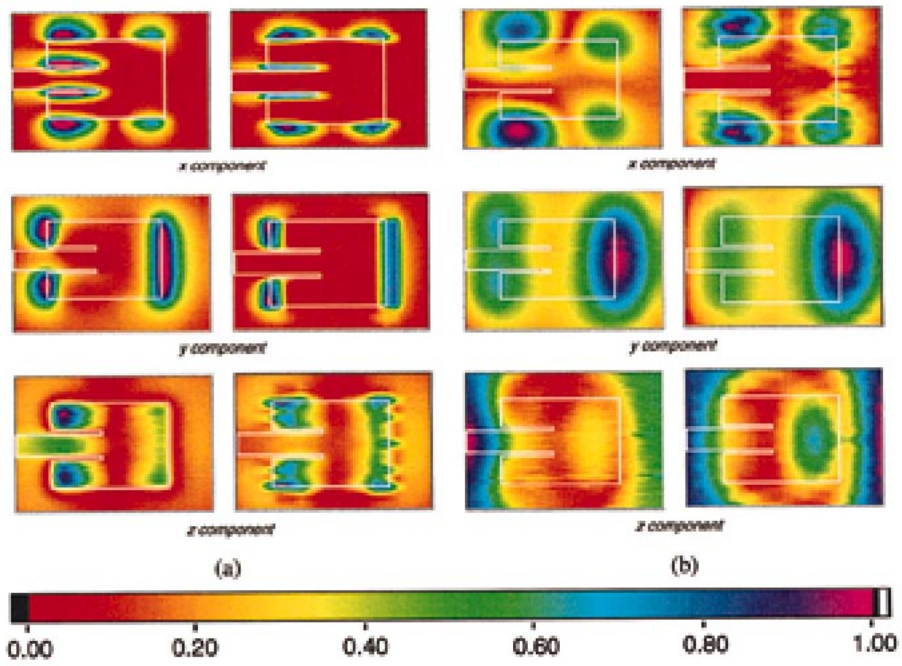

Fig. 2. Measured [first column of (a) and (b)] and simulated [second column of (a) and (b)] amplitude field patterns for three orthogonal components of the patch antenna at 4.003 GHz. The fields are normalized to the largest field amplitude in each plot. The perimeter of the antenna is indicated by the solid white line. (a) Measurement height: 0 mm (~ 100 μm). (b) Measurement height: 5.0 mm.

in both the x and y tangential directions can be observed around the edges of the patch and near the ends of the long dimension.

The z-component measurement result clearly displays the peak electric field around both near and far edges of the antenna (relative to the feed end). Since the z-component represents the normal field, the peak amplitude appears primarily over the metal of the antenna and near the edges. The x- and y-components (tangential fields), on the other hand, have their peak amplitudes outside the antenna pattern around the edges, where the probe captures the electric field as it becomes parallel to the plane of the patch.

The $LiTaO_3$ crystal probe is employed to capture both tangential components, although the two-directional sensitivity has been obtained in separate scans after rotating either the DUT or the probe by 90°. For the electric field x-component, the peak amplitudes are observed along the corners of the long side edges of the antenna and between the patch and matching-section insets. The four peaks around the corners of the antenna are explained by the potential distribution on the antenna, which is described at the start of this section. Due to the phase difference of the voltage between the feed line and the near-side edge of the antenna (as seen in Fig. 3), two amplitude peaks also occur at the impedance matching insets. For the y-component, the electrooptic field map measurement shows peak amplitudes on both the near- and far-side edges of the patch. These two y-component peak amplitudes also correspond well to the expected potential distribution on the antenna.

In order to verify the trends of the electrooptic measurements, a three-dimensional FEM simulation of the patch has been performed. The right-hand-side column of Fig. 2(a) shows the FEM simulation results at 0-mm height, right at the surface of the patch. For this FEM simulation, 183 816 mesh elements were

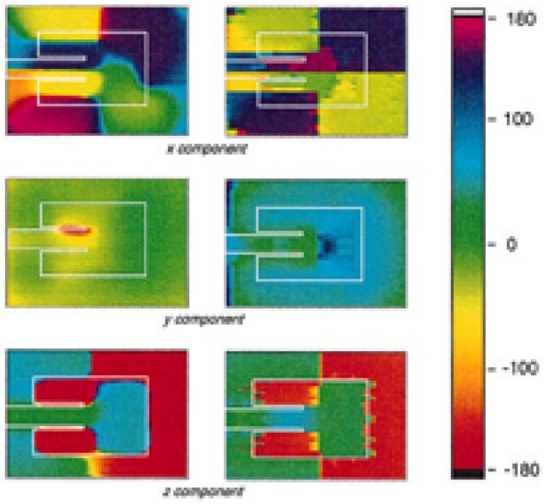

Fig. 3. Measured (left-hand side) and simulated (right-hand side) phase for three orthogonal field components of the patch antenna at 4.003 GHz and 0-mm height. The scale is in degrees.

used, and a calculation [central processing unit (CPU)] time of approximately 1.5 h with a Sun Ultra Sparc-2 workstation was necessary to produce one field map for the patch structure. All three field components show very good agreement between the simulation and measurement results. However, due to the limited memory capacity of the computer and the long processing time for the simulation, each tetrahedral mesh used in the simulation has a certain low-size limit. This limitation of the mesh size causes sampling errors. For instance, the simulation result for the z-component shows a relatively coarse field pattern due to the sampling error in the simulation. In comparison, the measurement field pattern from the electrooptic probe indicates a

much smoother more physically intuitive field pattern than the simulation.

B. Near- to Far-Field Transition Measurement

Fig. 2(b) shows the measurement and simulation results at a height of 5 mm from the patch surface. Again, each amplitude map is normalized to 1.0 independently of the other field components. The measurement result for the x-component shows a more broadened peak pattern than in Fig. 2(a) for 0-mm height. Due to the proximity of the two impedance-matching insets to each other, the peaks observed on the insets at 0-mm height, which are 180° out of phase, as seen in the phase maps of Fig. 3, rapidly cancel each other as the measurement height increases. As a result, the peaks on the insets are not observed at 5-mm height, while the other four peaks around the corners are still detectable. For the y-component, Fig. 2(a) shows equal peak amplitude on both the near- and far-side edges. However, as the measurement height increases, the peak located on the near-side edge decreases more rapidly than the peak on the far-side edge, as shown in Fig. 2(b). The y-component measurement result thus illustrates the transient state from the near- to far-field stage. Also, Fig. 2(b) shows a very uniform z-component field pattern at 5-mm height. Thus, we can conclude that the z-component has far less contribution than the x- or y-components as the measurement height increases. Both measurement and simulation results show excellent agreement for all three components.

From Figs. 2 and 3, each peak of the electric field in the x- and z-directions has an 180° phase difference with respect to its neighboring peaks. Due to these phase characteristics, the peak fields for the x- and z-components cancel each other at a relatively long distance from the antenna (i.e., the far field). As a consequence of the rapid field cancellations with height, the x- and z-components show a much quicker decrease than the y- component as the measurement height increases. In contrast, the two peaks of the electric field y-component are essentially in phase with each other. Thus, we can conclude that the y-component is the dominant field component for the patch antenna in the far-field condition.

To investigate the peak-value variation with height for each electric-field component, the field maxima are extracted from each of the two-dimensional mapping results and normalized to the maximum amplitude at 0-mm height. Fig. 4 shows the variation of the normalized peak electric-field values with respect to the measurement height. All three components show a monotonic decrease as the measurement height increases. However, the y-component exhibits a slower decrease up to the 5-mm height compared with the x- and z-components. Also, the y-component has a larger peak value compared with the x- and z-components beyond a height of 5 mm. The peak field variations from the three-dimensional FEM simulation results are presented along with those from the measurements in Fig. 4. Each component is normalized to the peak field value at 0 mm height independently of the other field components. Both the x- and z-components show very good agreement between the measurement and simulation results. However, the y-component shows a noticeable discrepancy between the simulation and measurement results. The discrepancy can be explained by

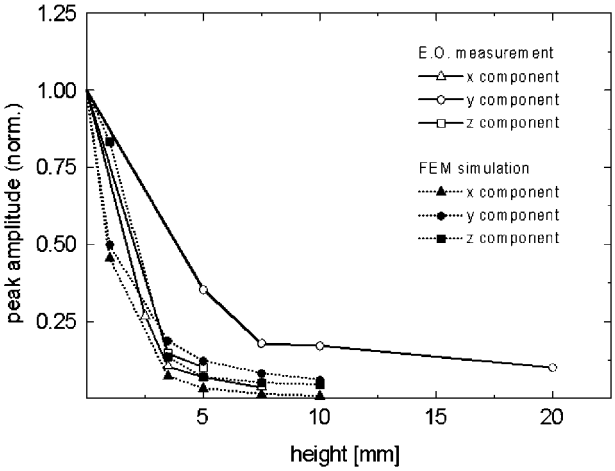

Fig. 4. Variation in peak electric field with respect to measurement height at 4.003 GHz. Each result is normalized to the maximum value at 0 mm, and the x-, y-, and z-components are normalized independently.

the imperfect absorbing boundary conditions during the simulation. It is practically impossible to handle infinite space in the simulation, thus, an absorbing boundary condition is employed to confine the simulation space. The ideal absorbing boundary condition cannot be obtained without knowing the exact field profile. Thus, we have to assume the resultant field profile before the simulation to set the absorbing boundary condition. However, the exact field profile can be acquired by the results of the simulation, given the ideal boundary conditions. This imperfection of the absorbing boundary condition causes errors between the real and calculated fields. In particular, the top boundary is more important than the other boundaries in the case of radiating structures (e.g., antennas). In the case of our 4-GHz patch, the x- and z-components decrease very rapidly as the height increases, while the y-component decreases more slowly. Thus, the imperfect absorbing boundary condition has more effect on the y-component than on the two other components. As a result, the y-component simulation result is inconsistent with the result from the measurement.

Fig. 5 shows the transition of the dominant field component (y-component) from the near to far field. The field maps are obtained at heights of 0.1, 1.0, 5.0, 7.5, and 10 mm. The measurement result at 1.0-mm height shows a very similar pattern as that at 0.1-mm height. However, the peak field at the edge opposite the feed end becomes dominant beyond 5-mm height. Also, the measurement results beyond 5-mm height show a more circularly shaped peak at the far-side edge. The transient patterns shown in Fig. 5 reveal that the peak electric field from the far-side edge of the patch provides the dominant contribution to the far-field radiation pattern.

C. S-Parameter Measurement

The electrooptic measurement technique has also been employed for the extraction of the scattering parameters of the microstrip patch antenna in an application that provides an alternative to conventional network analysis. This is potentially of great interest because the terahertz-bandwidth measurement capabilities of ultrafast-laser-based electrooptic sampling can lead

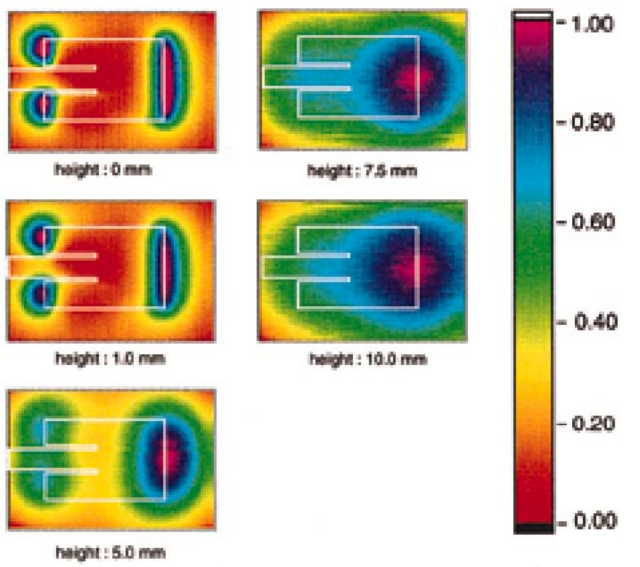

Fig. 5. Normalized measured amplitude variation from field maps, showing near- to far-field transition for dominant field component (y-component). Measurement plane height: 0, 1.0, 5.0, 7.5, and 10.0 mm.

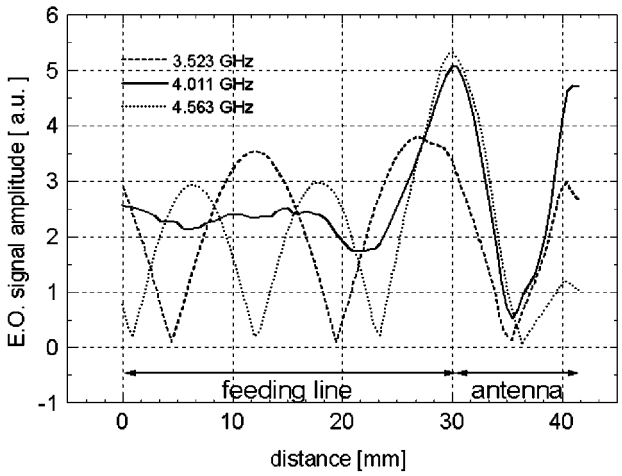

Fig. 6. Standing-wave amplitude measurement on the feed line and patch antenna at various operating frequencies at a measurement height of 200 μm. Dashed line: $f = 3.523$ GHz, solid line: $f = 4.011$ GHz (resonance frequency), dotted line: $f = 4.563$ GHz. The x-axis origin is where the center conductor of the coaxial cable meets the microstrip line. The lengths of the feeding line and antenna are indicated above the x-axis.

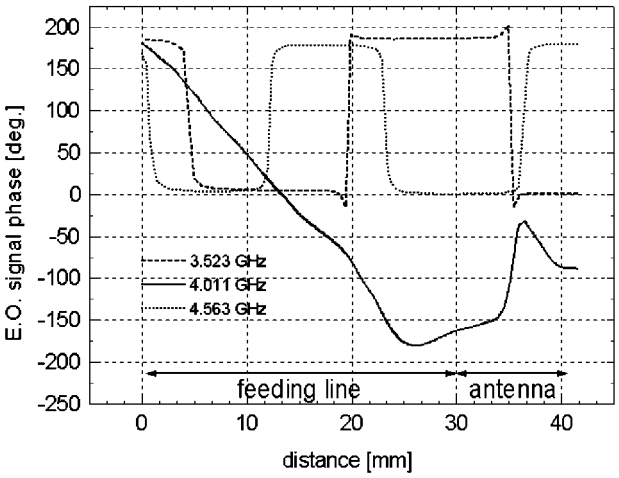

Fig. 7. Measured phase of the standing waves in degrees at a measurement height of 200 μm. Dashed line: $f = 3.523$ GHz, solid line: $f = 4.011$ GHz (resonance frequency), dotted line: f=4.563 GHz.

to very high-frequency optically based network analysis. In addition to the broad bandwidth capability of the electrooptic technique, the ability to measure directly on the DUT allows one to exclude the undesirable effects that occur between the RF source and DUT, such as the attenuation of the microwave cable and imperfect termination of the connectors. Since the microstrip antenna has only one port (input port), S_{11} is the sole relevant S-parameter. The S_{11} has thus been measured and also compared with the result obtained using the HP 8510B network analyzer.

To obtain the S_{11} of the microstrip patch, the relationship between the reflection coefficient and voltage standing-wave characteristic (VSWR) is used [14]. It is well known that the reflection coefficient γ is identical to the S_{11} if the system has a single port. One of the important characteristics of a transmission line is that the voltage and the electric-field relation are not changed unless the geometrical and electrical properties of the line are modified. Thus, along the microstrip feed line for our antenna, the field measured by the electrooptic probe has a direct correspondence to the voltage.

The electrooptic measurement technique has the capability to measure all three orthogonal electric-field components, as described above. Also, the patch antenna used in the measurement has a 50-Ω microstrip feed line, as shown in Fig. 1. By measuring one of the field components, we can calculate the VSWR on the feed line. However, due to the alignment of the antenna, the y-component is not detectable on the feed line [see Fig. 2(a)]. The normal electric field (z-component) has better uniformity across the feeding (x-direction) transmission line than the x-component, as observed in Fig. 2(a) and, thus, the z-component is used for the S-parameter measurement. One-dimensional electrooptic scanning is performed along the center of the feed line from the feeding point to the edge of the antenna using the BSO crystal probe. The measurement height is 200 μm. Fig. 6 shows measured standing-wave amplitude patterns at three different frequencies. At 3.523 GHz, the frequency is not sufficiently high for the resonance to exist. On the other hand, 4.563 GHz is beyond the resonance frequency. In both cases, the measurement results show a distinct standing-wave pattern on the feeding line. Two asymmetry peaks can also be observed at each edge of the antenna. At the resonance frequency (4.011 GHz), the measurement result shows that the standing-wave patterns on the feed line are vanishing, and the two symmetry peaks occur on both edges of the antenna.

Fig. 7 depicts the measured phase pattern on the feed line and patch antenna. The measurement results show typical standing-wave phase characteristics for both 3.523- and 4.563-GHz frequencies. Each point where the phase changes by 180° in Fig. 7 is coincident with a minimum amplitude point in Fig. 6. However, the phase appears to have the property of a traveling wave when the antenna is operated at its resonance frequency. The results show that most of the input signal is reflected back from the antenna when the antenna is operated

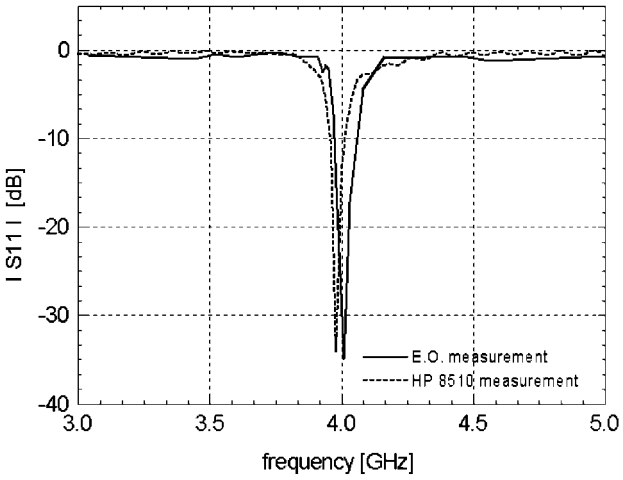

Fig. 8. Magnitude of S_{11} parameters of the microstrip patch antenna in decibels. Dashed line: HP 8510 network analyzer result, solid line: electrooptic measurement result.

under the off-resonance conditions. On the contrary, good signal propagation is observed on the feed line at the resonance frequency. From the result, we can conclude that most of the input signal is radiated from the antenna under the resonance frequency condition. Finally, $|S_{11}|$ of the antenna can be obtained from the measured data under the assumption that the feed line has very small loss. Fig. 8 shows the resultant $|S_{11}|$ along with the result obtained using an HP 8510 network analyzer. The results show excellent agreement with each other.

During conventional network analyzer measurements, it is almost impossible to calibrate out certain factors such as the imperfect connection between the center conductor of the coaxial cable and microstrip line. Herein lies a tremendous advantage for the use of electrooptic sampling for network analysis. That is, the electrooptic technique allows one to determine the pure electric field that exists on the feed line and antenna, in this case, without worrying about the mismatch or loss of external cables and connectors. This difference between the two methods likely explains the slight disagreement in the two resonance frequencies presented in Fig. 8.

IV. Conclusion

Three-dimensional electrooptic field mapping of a microstrip patch-antenna structure is performed for a complete set of three orthogonal electric-field components. The technique makes it possible to accurately determine the near-field radiation pattern of an antenna array, as well as the dominant field component of the patch-antenna structure. Also, the capability for detecting the near- to far-field transition is demonstrated. The three-dimensional measurement results are compared with FEM simulation results, making clear that the electrooptic measurement can provide superior results to the simulation. Also, the forward scattering parameter S_{11} is calculated from the electrooptic measurement of the standing-wave pattern on the feed line and antenna based on the normal-field measurement result. The result obtained from the electronic network analyzer shows an almost identical S_{11} pattern. Due to the capability of measuring electric fields directly on a microwave structure, the demonstrated electrooptic method can minimize effects that are otherwise very difficult to calibrate out during network analyzer measurements, including imperfect feeding and electrical contact. In conclusion, electrooptic field mapping is a very powerful tool for the analysis and design of microwave radiating structures, such as single antenna elements or radiating arrays.

References

[1] A. D. Yaghijian, "An overview of near-field antenna measurements," *IEEE Trans. Antennas Propagat.*, vol. AP–34, pp. 30–45, Jan. 1986.

[2] T. Budka, S. D. Waclawick, and G. Rebeiz, "A coaxial 0.5–18 GHz near electric field measurement system for planar microwave circuits using integrated probes," *IEEE Trans. Microwave Theory Tech.*, vol. 44, pp. 2174–2183, Dec. 1996.

[3] Y. Gao and I. Wolff, "A new miniature magnetic field probe for measuring three-dimensional fields in planar high frequency circuits," *IEEE Trans. Microwave Theory Tech.*, vol. 44, pp. 911–918, Dec. 1996.

[4] J. Valdmanis and G. Mourou, "Subpicosecond electrooptic sampling: Principles and applications," *IEEE J. Quantum Electron.*, vol. QE-22, pp. 69–78, Jan. 1986.

[5] B. H. Kolner and D. M. Bloom, "Electrooptic sampling in GaAs integrated circuits," *IEEE J. Quantum Electron.*, vol. QE-22, pp. 79–93, Jan. 1986.

[6] M. G. Li, E. A. Chauchard, C. H. Lee, and H.-L. A. Hung, "Two-dimensional field mapping of GaAs microstrip circuit by electrooptic sensing," in *OSA Proc. Picosecond Electron. Optoelectron.*, Salt Lake City , UT, Mar. 1991, pp. 54–58.

[7] G. David, S. Redlich, W. Mertin, R. M. Bertenburg, S. Koßlowski, F. J. Tegude, and D. Jäger, "Two-dimensional direct electro-optic field mapping in a monolithic integrated GaAs amplifier," in *Proc. 23rd EuMC*, Madrid, Spain, Sept. 1993, pp. 497–499.

[8] G. David, R. Tempel, I. Wolff, and D. Jäger, "Analysis of microwave propagation effects using 2D electro-optic field mapping techniques," *Opt. Quantum Electron.*, vol. 28, pp. 919–931, July 1996.

[9] K. Yang, G. David, S. Robertson, J. F. Whitaker, and L. P. B. Katehi, "High resolution electro-optic mapping of near-field distributions in integrated microwave circuits," in *IEEE MTT-S Int. Microwave Symp. Dig.*. New York, June 1998, pp. 949–962.

[10] K. Kamogawa, I. Toyoda, K. Nishikawa, and T. Tokumitsu, "Characterization of a monolithic slot antenna using an electro-optic sampling technique," *IEEE Microwave Guided Wave Lett.*, vol. 4, pp. 414–416, Dec. 1994.

[11] T. Pfeifer, T. Loeffler, H. G. Roskos, H. Kurz, M. Singer, and E. M. Bieble, "Electro-optic near-field mapping of planar resonators," *IEEE Trans. Antennas Propagat.*, vol. 46, pp. 284–291, Feb. 1998.

[12] J. F. Whitaker, J. A. Valdmanis, M. Y. Frankel, S. Gupta, J. Chwalek, and G. A. Mourou, "External electro-optic integrated circuit probing," *Microelectron. Eng.*, vol. 12, pp. 369–379, 1990.

[13] J. A. Valdmanis, "Electro-optic measurement techniques for picosecond materials, devices, and integrated circuits," in *Measurement of High-Speed Signals in Solid State Devices*, R. B. Marcus, Ed. New York: Academic, 1990, pp. 136 –219.

[14] D. M. Pozar, *Microwave Engineering*. Reading, MA: Addison-Wesley, 1990.

Kyoung Yang (S'90) was born in Seoul, Korea. He received the B.S. and M.S. degrees in electrical engineering from Seoul National University, Seoul, Korea, in 1990 and 1993, respectively, and is currently working toward the Ph.D. degree in electrical engineering and computer science at The University of Michigan at Ann Arbor.

His current research interests include the development of the high-speed electrooptic and photo-conductive measurement technique for the characterization of microwave and millimeter-wave circuits and radiators.

Gerhard David (M'97), photograph and biography not available at time of publication.

Jong-Gwan Yook (S'89–M'89) was born in Korea. He received the B.S. and M.S. degrees in electronic engineering from Yonsei University, Seoul, Korea, in 1987 and 1989, respectively, and the Ph.D. degree from The University of Michigan at Ann Arbor, in 1996.

He is currently an Assistant Professor at the Kwang-Ju Institute of Science and Technology (K-JIST), Kwang-Ju, Korea. His main research interests are in the area of theoretical/numerical electromagnetic modeling and characterization of microwave/millimeter-wave circuits and components and VLSI and monolithic-microwave integrated-circuit (MMIC) interconnects using frequency- and time-domain full-wave methods, and development of numerical techniques for analysis and design of high-speed high-frequency circuits with emphasis on parallel/super computing and wireless communication applications.

Ioannis Papapolymerou, photograph and biography not available at time of publication.

Linda P. B. Katehi (S'81–M'84–SM'89–F'95) received the B.S.E.E. degree from the National Technical University of Athens, Athens, Greece, in 1977, and the M.S.E.E. and Ph.D. degrees from the University of California at Los Angeles, in 1981 and 1984, respectively.

In September 1984, she joined the faculty of the Electrical Engineering and Computer Science Department, The University of Michigan at Ann Arbor, where she is currently an Associate Dean for Graduate Education and a Professor of electrical engineering and computer science. She has been interested in the development and characterization (theoretical and experimental) of microwave, millimeter printed circuits, the computer-aided design of VLSI interconnects, the development and characterization of micromachined circuits for millimeter-wave and submillimeter-wave applications, and the development of low-loss lines for terahertz-frequency applications. She has also been theoretically and experimentally studying various types of uniplanar radiating structures for hybrid and monolithic circuits, as well as monolithic oscillator and mixer designs.

Dr. Katehi is a member of Sigma XI, Hybrid Microelectronics, URSI Commission D, the IEEE Antennas and Propagation Society (IEEE AP-S), the IEEE Microwave Theory and Techniques Society (IEEE MTT-S), and the IEEE AP-S AdCom (1992 to 1995). She was awarded the 1984 IEEE AP-S W. P. King (Best Paper Award for a Young Engineer), the 1985 IEEE AP-S S. A. Schelkunoff Award (Best Paper Award), the 1987 NSF Presidential Young Investigator Award, a 1987 URSI Young Scientist Fellowship, the 1994 Humboldt Research Award, the 1994 University of Michigan Faculty Recognition Award, the 1996 IEEE MTT-S Microwave Prize, and the 1997 Best Paper Award presented by the International Society on Microelectronics and Advanced Packaging. She is an associate editor for the IEEE TRANSACTIONS ON MICROWAVE THEORY AND TECHNIQUES.

John F. Whitaker (S'84–M'88) received the B.Sc. degree in physics from Bucknell University, Lewisburg, PA, in 1981, and the M.Sc. and Ph.D. degrees in electrical engineering from the University of Rochester, Rochester, NY, in 1983 and 1988, respectively.

In 1989, he joined the faculty of the Department of Electrical Engineering and Computer Science, The University of Michigan at Ann Arbor. He is currently a Research Scientist and Adjunct Associate Professor and the Coordinator of the Ultrafast Technology Area in the National Science Foundation Center for Ultrafast Optical Science. In 1995, he was appointed Visiting Professor, First Class at the University of Savoie, Savoie, France. His research interests involve ultrafast-response optoelectronic materials, devices, and test and characterization techniques, as well as guided and free-space-radiating terahertz-bandwidth pulses.

Dr. Whitaker is a member of the IEEE Microwave Theory and Techniques Society (IEEE MTT-S) and the IEEE Lasers and Electro-Optics Society (IEEE LEOS). He is currently chair of the IEEE LEOS Technical Committee on Ultrafast Optics and Electronics. He was a recipient of the 1996 Microwave Prize presented by the IEEE MTT-S, and has received the Research Excellence Award presented by the Department of Electrical Engineering and Computer Science, The University of Michigan at Ann Arbor, and the Outstanding Research Scientist Achievement Award from the College of Engineering, The University of Michigan at Ann Arbor.